

# Dose-optimized HILT promotes peripheral nerve repair through BMP4-Smad9-mediated inhibition of neuroinflammation and oxidative stress

Cite as: APL Bioeng. **10**, 016115 (2026); doi: 10.1063/5.0289844

Submitted: 9 July 2025 · Accepted: 24 February 2026 ·

Published Online: 5 March 2026



Lanlan Gong,  Danyang Li, Xiaojing Zhao, Yujuan Qu, Shasha Song, Jialin Liu, and Shouwei Yue<sup>a)</sup> 

## AFFILIATIONS

Rehabilitation Center, Qilu Hospital of Shandong University, Jinan, Shandong, China

<sup>a)</sup> Author to whom correspondence should be addressed: [shouweiy@sdu.edu.cn](mailto:shouweiy@sdu.edu.cn)

## ABSTRACT

Evidence has shown that high-intensity laser therapy (HILT) may be beneficial for recovery after peripheral nerve injury (PNI). However, the optimized doses and effective mechanisms remain unclear. The present study sought to explore the effects of various doses of HILT on the recovery of nerve function in sciatic nerve injury (SNI) rats. The potential mechanism of action of HILT alleviating PNI was also assessed. Behavioral testing, polymerase chain reaction, immunoblotting, and immunofluorescence analyses were applied to explore whether HILT promotes the repair of injured nerves and its underlying mechanisms. SNI induces mechanical nociceptive hypersensitivity, disrupts sciatic nerve structure and function, causes gastrocnemius muscle atrophy, and increases oxidative stress and expression levels of inflammatory factors. HILT effectively ameliorated these SNI-induced alterations. Notably, the Bone Morphogenetic Protein 4 (BMP4)-SMAD Family Member 9 (Smad9) pathway mediates the therapeutic effects of HILT on SNI repair. These findings show for the first time that HILT stimulates the BMP4-Smad9 signaling pathway by increasing Smad9 expression to regulate inflammation and oxidative stress, which ultimately ameliorates SNI.

© 2026 Author(s). All article content, except where otherwise noted, is licensed under a Creative Commons Attribution (CC BY) license (<https://creativecommons.org/licenses/by/4.0/>). <https://doi.org/10.1063/5.0289844>

## INTRODUCTION

Peripheral nerve injury (PNI) leads to persistent motor and sensory dysfunction and remains a major clinical challenge due to slow and often incomplete functional recovery.<sup>1–3</sup> However, the clinical outcomes of existing treatment strategies remain unsatisfactory.<sup>4–14</sup> Although the peripheral nervous system retains a limited capacity for regeneration,<sup>15</sup> spontaneous repair is typically insufficient to restore full neuromuscular function, highlighting the need for effective therapeutic interventions.<sup>16</sup>

High-intensity laser therapy (HILT) is a type of physical factor therapy for various illnesses.<sup>17</sup> Recent evidence has shown that HILT has emerged as a promising noninvasive modality for neuromuscular rehabilitation and pain management.<sup>18–21</sup> Unlike low-level photobiomodulation, HILT enables deeper tissue penetration and higher energy delivery, making it particularly attractive for treating peripheral nerve lesions. However, the therapeutic efficacy of HILT is highly dependent on irradiation parameters, and the absence of optimized dose windows and mechanistic validation has substantially limited its translational application in peripheral nerve repair.<sup>18</sup>

Based on these findings, the present study aims to elucidate the precise mechanisms by which HILT mitigates PNI. Two principal pathophysiological pathways have been identified in the pathogenesis of PNI: inflammation and oxidative stress.<sup>22–24</sup> Traumatic injury to peripheral nerves can result in neuroinflammation, which is triggered by the fragmentation of the extracellular matrix (ECM), the secretion of interleukins (ILs) and cytokines, and the accumulation of stimulated immune cells.<sup>25–27</sup> After PNI, the antioxidant defenses on the side of the injury are insufficient to eliminate reactive oxygen species and other cell-generated free radicals that damage tissues surrounding the injury.<sup>28</sup> Several studies have explored the potential of anti-inflammatory and antioxidant therapies for PNI,<sup>29–31</sup> however, their precise molecular mechanisms remain incompletely elucidated. It is, therefore, possible that the prevention of PNI-induced inflammation and oxidative stress may represent a viable therapeutic target for PNI patients, necessitating further mechanistic exploration to guide clinical translation.

Recent studies have demonstrated that the Bone Morphogenetic Protein 4 (BMP4)-SMAD Family Member 9 (Smad9) pathway is

critically involved in the regulation of inflammation and oxidative stress.<sup>32,33</sup> Furthermore, evidence indicates that the BMP4-Smad9 signaling pathway plays a critical role in promoting corneal tissue repair,<sup>34</sup> with emerging evidence suggesting its regulatory effects on osteogenic factor secretion.<sup>35</sup> However, its functional implications in neural regeneration and repair remain unknown. Consequently, further investigation of the BMP4-Smad9 signaling axis, particularly its mechanistic involvement in HILT-mediated PNI recovery, is scientifically justified. This line of inquiry is justified and holds considerable potential for clinical translation and application value, as it may

unveil novel therapeutic targets for optimizing neuromodulatory interventions.

**RESULTS**

**HILT facilitates the restoration of motor function following SNI**

After creating a model of a crushed nerve, rats were administered HILT 5 days a week for 4 weeks to evaluate the effect of HILT on the rehabilitation of motor function [Fig. 1(a)]. The Sciatic function indexes (SFI) was utilized to assess motor functional recovery.

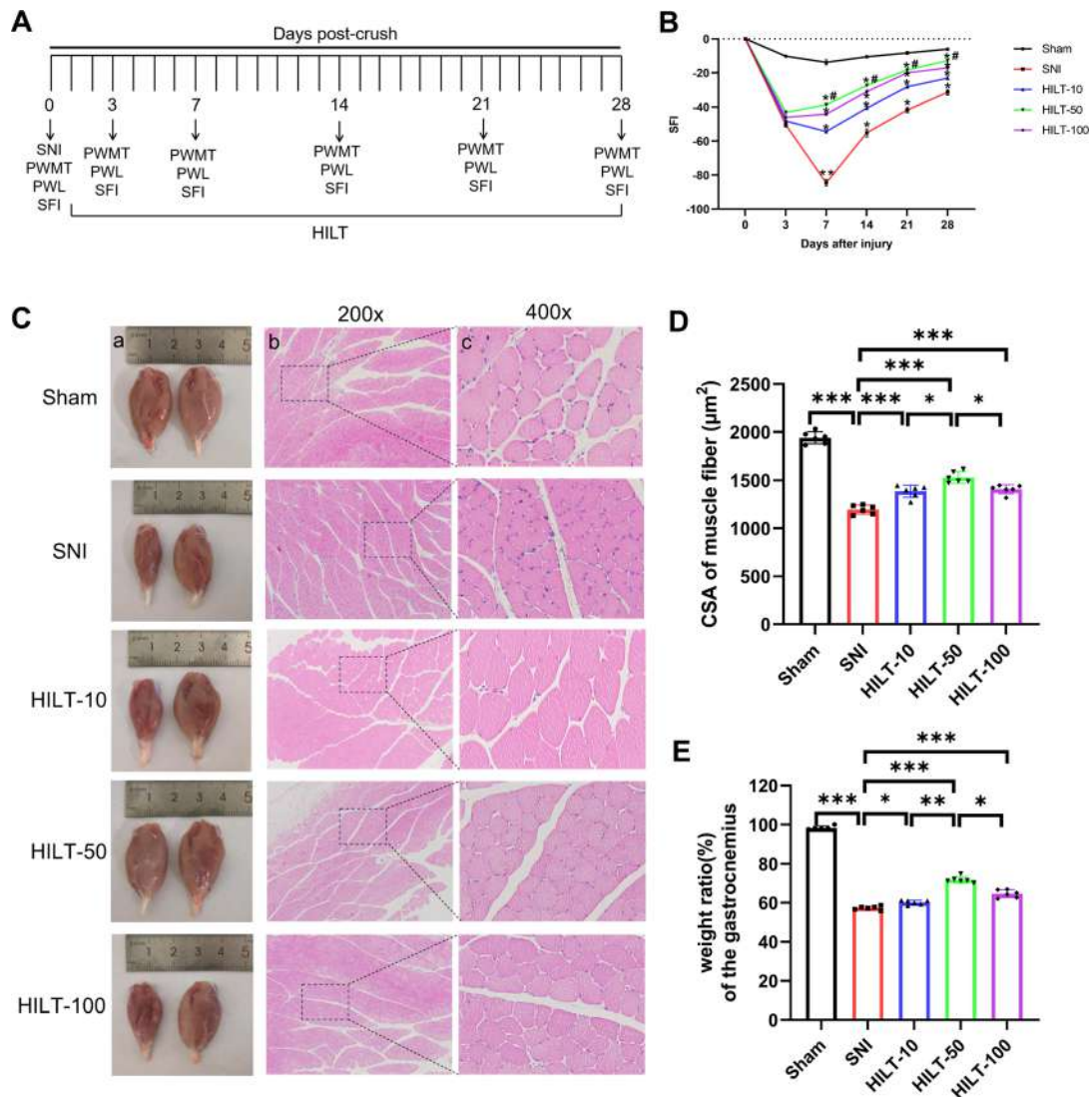


**FIG. 1.** HILT promotes recovery of motor function after SNI. (a) Flow chart for experiment. (b) SFI was employed to assess functional recovery after injury and HILT. \* $p < 0.05$ , \*\* $p < 0.01$  vs Sham group; # $p < 0.05$  vs SNI group. (c) Morphology of bilateral gastrocnemius muscles on postoperative day 28 and morphology of H&E-stained muscle fibers in cross section. (d) Comparison of mean cross-sectional area (CSA) of gastrocnemius cells on the 28th day after operation. (e) On the 28th day following surgery, the bilateral gastrocnemius wet weight ratios in each group were compared. HILT-10, HILT-50, and HILT-100 denote cumulative fluence of 10, 50, and 100 J/cm<sup>2</sup> delivered to the scanned treatment area, respectively. Results are expressed as means  $\pm$  standard deviation (SD) ( $n = 6$ ). \* $p < 0.05$ , \*\* $p < 0.01$ , and \*\*\* $p < 0.001$ . Repeated measurements ANOVA, followed by Tukey's *post hoc* tests to determine  $p$  value in panel B, and one-way ANOVA followed by Tukey's *post hoc* tests to determine  $p$  value in panels D and E. These findings identify that moderate-dose HILT promotes muscle functional and structural recovery after nerve injury.

Walking track analysis was applied to assess the effects of HILT on peripheral nerve healing via the inspection of the SFIs of rats at predetermined intervals. All injury groups showed a significant decline in SFI scores at day 3 post-operation, indicating the successful establishment of the injury model. Treatment effects began to emerge at weeks 1–2, as evidenced by some recovery in the SFI scores across all treatment groups. However, the notable improvements were observed from week 3 onward, and the HILT-50 group showed particularly marked recovery, with SFI scores approaching Sham group levels, while the other treatment groups (HILT-10 and HILT-100) exhibited more modest improvements [Fig. 1(b)]. This dose-dependent response suggests a critical therapeutic window for HILT-mediated neuromodulation. The gastrocnemius of both hind limbs was removed on day 28 after surgery, and the wet weight ratio was examined. The gastrocnemius on the damaged side was significantly smaller than that on the opposite side in all groups, except for the Sham group. A significant difference in the wet weight of the gastrocnemius was found in the sciatic nerve injury (SNI) group, while there was a smaller difference in the wet weight in three HILT groups, especially the HILT-50 group [Figs. 1(c) and 1(e)]. At 4 weeks postoperatively, target muscle morphometry showed different degrees of atrophy in crush groups, with the HILT-50 group exhibiting the best recovery of muscle [Figs. 1(c) and 1(d)].

### HILT promotes the regeneration of nerves after SNI

A complex series of processes, such as neural membrane growth, myelin degeneration, and axonal necrosis, occur in the distal portion of the nerve after PNI. The stereotyped process of degenerative events that occurs in the distal axon after injury is known as Wallerian degeneration. Western blotting of GAP43 and S100 $\beta$  was performed for assessment of axon growth. As shown in Figs. 2(a)–2(c), the levels of the indicators were higher in the three HILT groups than in the SNI group, with the HILT-50 group exhibiting the highest expression levels. Similarly, the protein expression of GAP43 and S100 $\beta$ , measured by immunofluorescence staining, further confirmed the pro-neural regenerative role of HILT [Figs. 2(d)–2(f)]. To determine histologic alterations following SNI and rehabilitation, pathological changes in the sciatic nerve tissues were assessed in all groups of rats on day 28 after the start of the model [Fig. 2(d)]. Toluidine blue staining and transmission electron microscopy (TEM) showed that, compared to the SNI group, the three HILT treatment groups exhibited higher axon density, thicker myelin sheaths, and smaller g-ratios, with the HILT-50 group showing the most pronounced effects [Fig. 2(d), Table I]. These structural improvements correlated with functional recovery, as evidenced by allodynia assessments: HILT-50 normalized paw withdrawal mechanical threshold (PWMT) and paw withdrawal latency (PWL) to near-sham levels by postoperative day 28 [Figs. 2(g) and 2(h)].

### HILT inhibits SNI-induced inflammatory response and oxidative stress in rats

After SNI, the tissue undergoes an inflammatory response. The expression level of inflammatory factors was detected to explore the effect of HILT on the inflammatory response in SNI rats. HILT-50 was selected as the experimental dose. Real-time quantitative polymerase chain reaction (RT-qPCR) showed that HILT strongly suppressed the

SNI-induced increase in tumor necrosis factor alpha (TNF- $\alpha$ ), Interleukin-1beta (IL-1 $\beta$ ), and Interleukin-6 (IL-6) expression [Figs. 3(a)–3(c)]. Immunofluorescence staining for TNF- $\alpha$ , IL-1 $\beta$ , and IL-6 was conducted to further assess the inflammatory response in the sciatic nerve. Likewise, HILT significantly reduced the production of inflammatory cytokines induced by SNI [Figs. 3(d)–3(g)]. nicotinamide adenine dinucleotide phosphate (NADPH) oxidase 4 (NOX4) is one of the main isoforms of nicotinamide adenine dinucleotide phosphate (NADPH). Our data showed that HILT reversed the SNI-induced increase in NOX4 [Figs. 3(h) and 3(i)]. Superoxide dismutase (SOD) is a vital component of redox state balance, which is essential for maintaining homeostasis in the nervous system. Its activity may serve as an indirect indicator of the body's capacity to eliminate free radicals. Superoxide dismutase 2 (SOD2) levels exhibited a significant decrease following SNI, whereas they were elevated by HILT [Figs. 3(h) and 3(j)]. One of the byproducts of the lipid peroxidation chain reaction is malondialdehyde (MDA). An elevated level of MDA serves as a proxy for the degree of cellular damage caused by free radicals. It was found that HILT also attenuated the increase in MDA after SNI [Fig. 3(k)].

### HILT activates BMP4-Smad9 pathway in SNI rats

To investigate the role of the BMP4-Smad9 pathway in HILT-mediated amelioration of SNI, we quantified the expression levels of BMP4, p-Smad1/5/9, and Smad9 in the sciatic nerves of rats across experimental groups [Figs. 4(a)–4(d)]. Western blotting analysis revealed that the expression levels of BMP4, p-Smad1/5/9, and Smad9 proteins were significantly decreased following SNI, whereas HILT treatment effectively upregulated their expression. These results were validated using immunofluorescence staining [Figs. 4(e)–4(g)] and RT-qPCR [Figs. 4(h) and 4(i)]. The findings demonstrated that following SNI, BMP4, p-Smad1/5/9, and Smad9 expression levels were markedly lower, which were elevated after HILT treatment.

### Overexpression of Smad9 attenuates the inflammation and oxidative stress induced by SNI

Subsequently, we investigated the effect of the BMP4-Smad9 pathway on neuroinflammation, oxidative stress, and nerve repair. Smad9 overexpression was achieved using adeno-associated virus (AAV) [Figs. 5(a)–5(c)]. The AAV-Smad9 groups exhibited significantly lower NOX4 contents and higher SOD2 contents than the AAV-nc groups [Figs. 5(d)–5(f)]. Overexpression of Smad9 reverses SNI-induced increase in MDA levels [Fig. 5(g)]. Results showed that Smad9 overexpression dramatically suppressed SNI-induced elevation of IL-6, IL-1 $\beta$ , and TNF- $\alpha$  expression, suppressing the inflammatory response [Figs. 5(h)–5(j)]. Furthermore, the repair of the sciatic nerve was evaluated by PWMT, PWL, and SFI. As anticipated, overexpression of Smad9 increases PWMT and PWL values [Figs. 5(k) and 5(l)]. Also, the SFI of rats gradually improved after Smad9 overexpression [Fig. 5(m)].

### HILT promotes nerve injury repair through the BMP4-Smad9 pathway

LDN193189 (LDN) has been shown to act as an inhibitor of the BMP-Smad pathway; therefore, we used it to confirm the protective effect of HILT on injured nerves [Figs. 6(a)–6(d)]. LDN significantly

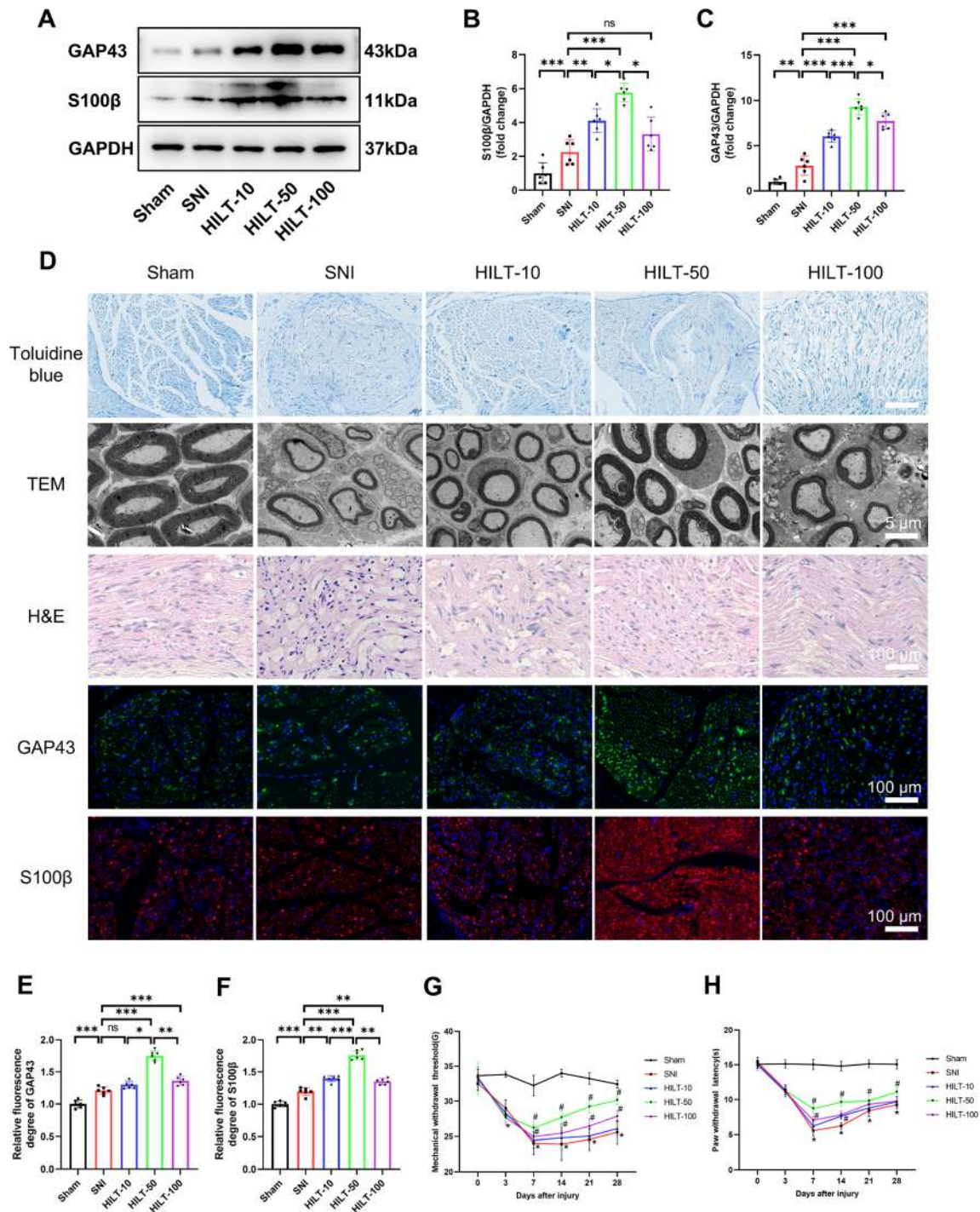


**FIG. 2.** HILT promotes nerve regeneration after SNI. (a)–(c) GAP43 and S100β expression in the sciatic nerve tissues from each group was measured using Western blotting. (d) Five images of varying types for each group, including images of toluidine blue staining, TEM, H&E staining, and GAP43 and S100β staining for cross sections of the regenerative sciatic nerve tissue (4 weeks). Scale bar = 100 μm. (e) and (f) Quantitative analysis of GAP43 and S100β immunofluorescence images. (g) and (h) Calculating PWMT and PWL on days 0, 3, 7, 14, 21, and 28 following SNI surgery in rats (\**p* < 0.05 vs Sham group; #*p* < 0.05 vs SNI group). \**p* < 0.05, \*\**p* < 0.01, \*\*\**p* < 0.001, ns denotes no significance, and *n* = 6 in each group. One-way ANOVA followed by Tukey's *post hoc* tests to determine *p* value in panels B, C, E, and F, and repeated measurements ANOVA, followed by Tukey's *post hoc* tests to determine *p* value in panels G and H. This identifies that HILT promotes axonal regeneration and remyelination, which underlies the restoration of sensory and motor function.

**TABLE I.** Histomorphometric parameter analysis of toluidine blue staining and TEM of sciatic nerves in each group.

Group	Axon density (Axons/mm <sup>2</sup> )	Thickness of myelin ( $\mu$ m)	G-ratio
Sham	18 497.60 $\pm$ 1541.00	1.16 $\pm$ 0.19	0.64 $\pm$ 0.04
SNI	4883.00 $\pm$ 824.54*	0.35 $\pm$ 0.06*	0.80 $\pm$ 0.02*
HILT-10	8137.53 $\pm$ 1451.32 <sup>#</sup>	0.52 $\pm$ 0.09	0.76 $\pm$ 0.03
HILT-50	14 178.33 $\pm$ 1465.76 <sup>#,\$</sup>	0.97 $\pm$ 0.10 <sup>#,\$</sup>	0.69 $\pm$ 0.01 <sup>#,\$</sup>
HILT-100	9436.39 $\pm$ 1297.16 <sup>†</sup>	0.58 $\pm$ 0.06 <sup>†</sup>	0.74 $\pm$ 0.02 <sup>†</sup>

Data were presented as mean  $\pm$  SD and analyzed with one-way ANOVA followed by Tukey's *post hoc* test. SNI: sciatic nerve injury; HILT-10: high-intensity laser therapy 10 J/cm<sup>2</sup>; HILT-50: high-intensity laser therapy 50 J/cm<sup>2</sup>, and HILT-100: high-intensity laser therapy 100 J/cm<sup>2</sup>. \**p* < 0.05 vs Sham group; <sup>#</sup>*p* < 0.05 vs SNI group; <sup>\$</sup>*p* < 0.05 vs HILT-10 group; <sup>†</sup>*p* < 0.05 vs HILT-50 group.

reversed NOX4 downregulation and SOD2 downregulation in HILT-treated sciatic nerves [Figs. 6(e)–6(g)]. Simultaneously, HILT-induced downregulation of MDA and inflammatory factors was reversed by LDN [Figs. 6(h)–6(k)]. Tests of PWMT, PWL, and SFI reveal that LDN attenuates HILT's facilitation of neurologic function [Figs. 6(l)–6(n)], suggesting that LDN partially reduces the protective effect of HILT on injured nerves, functionally linking BMP-Smad activation to HILT's pro-regenerative outcomes.

### Overexpression of Smad9 inhibits TNF- $\alpha$ -induced oxidative stress and inflammatory responses in SCs

The process of regeneration following PNI is typically attributed to the proliferation of Schwann cell (SC). Being crucial cells for the peripheral nervous system's structure and function, SCs recruit and work concertedly with macrophages to eradicate degenerating myelin segments and axons. Meanwhile, SCs create bands that aid in axon development during regeneration. Consequently, one intriguing tactic to promote axonal regeneration may be the manipulation of SCs. Therefore, we hypothesized that Smad9 overexpression would affect SC, so we transfected SC with a plasmid containing Smad9 to increase p-Smad1/5/9 and Smad9 expression [Figs. 7(a)–7(c)]. Reduced level of MDA, decreased expression of NOX4, and increased expression of SOD2 confirmed that overexpression of Smad9 inhibited oxidative stress in the SCs [Figs. 7(d)–7(g)]. Immunofluorescence and PCR assays showed that Smad9 overexpression reduced the levels of inflammatory factors [Figs. 7(h)–7(k)], suggesting that Smad9 overexpression inhibited the inflammatory response in SCs.

## DISCUSSION

Our study has demonstrated that HILT promotes functional and structural recovery after SNI by modulating the BMP4-Smad9 signaling pathway. Our key findings demonstrate that HILT, particularly at a moderate dose of 50 J/cm<sup>2</sup> (HILT-50), optimally ameliorates SNI-induced motor and sensory deficits, muscle atrophy, and neuroinflammation. Furthermore, we establish that the therapeutic effects of HILT are mechanistically linked to the activation of the BMP4-Smad9 pathway within the sciatic nerve and SCs, and that this activation directly regulates the inflammatory and oxidative stress responses (Fig. 8). These findings suggest that the BMP4-Smad9 signaling pathway may represent an important underlying mechanism for the therapeutic effects of HILT in neurological damage, expanding the molecular understanding of photobiomodulation.

As a reintegration method, HILT has shown improvements in the recovery of PNI in recent years.<sup>36,37</sup> While the efficacy of HILT has been reported with some variability in the literature,<sup>38,39</sup> our study provides a clear mechanistic rationale for its role in nerve repair. The discrepancy could be attributed to our use of a specific high-intensity Nd:YAG laser (1064 nm) and the carefully standardized energy densities, which allow for deeper tissue penetration and more potent biologic effects.<sup>40</sup> The observed dose-dependent efficacy, with HILT-50 yielding optimal outcomes, aligns with the concept of biphasic dose response in photobiomodulation, where biological stimulation peaks at a specific energy range before declining at higher doses.<sup>41</sup> This underscores the importance of parameter optimization in clinical translation. Our inclusion of a high-dose group (HILT-100) confirms that exceeding the therapeutic window does not enhance recovery, consistent with previous findings.<sup>42</sup> Although thermal effects cannot be entirely excluded in any form of laser irradiation, several lines of evidence suggest that the therapeutic outcomes observed in this study are unlikely to be driven by heat accumulation. First, the Nd:YAG HILT protocol used here closely matches those reported in prior studies that documented negligible surface temperature elevation and the absence of histological thermal damage.<sup>43</sup> Second, according to bioheat transfer theory and reported tissue optical properties at 1064 nm, the predicted temperature increase under our experimental conditions remains below 1–2 °C, which is far below the threshold required to induce thermal injury or protein denaturation.<sup>44</sup> Collectively, these considerations suggest that the therapeutic effects are primarily attributable to photobiomodulatory mechanisms; however, thermal contributions cannot be fully excluded in the absence of direct temperature monitoring. While the focus of this study is on the biological and molecular effects of HILT, the combination of standardized surface delivery, parameter selection, and literature-supported light transport estimates provides a reasonable engineering approximation linking applied dose to target-tissue exposure.<sup>45</sup> Such an approach is consistent with prior studies where direct subsurface measurements are impractical. To rule out potential nonspecific effects of laser irradiation on neural function, we included a Sham + HILT control group in our behavioral analyses. We found no significant differences in SFI, PWMT, or PWL between the Sham and Sham + HILT groups (supplementary material Fig. 1), confirming that the observed recovery in SNI + HILT animals is a specific therapeutic response to injury rather than a general stimulation.

Having established the therapeutic window and specificity of HILT, we sought to delineate its underlying mechanism. A central and

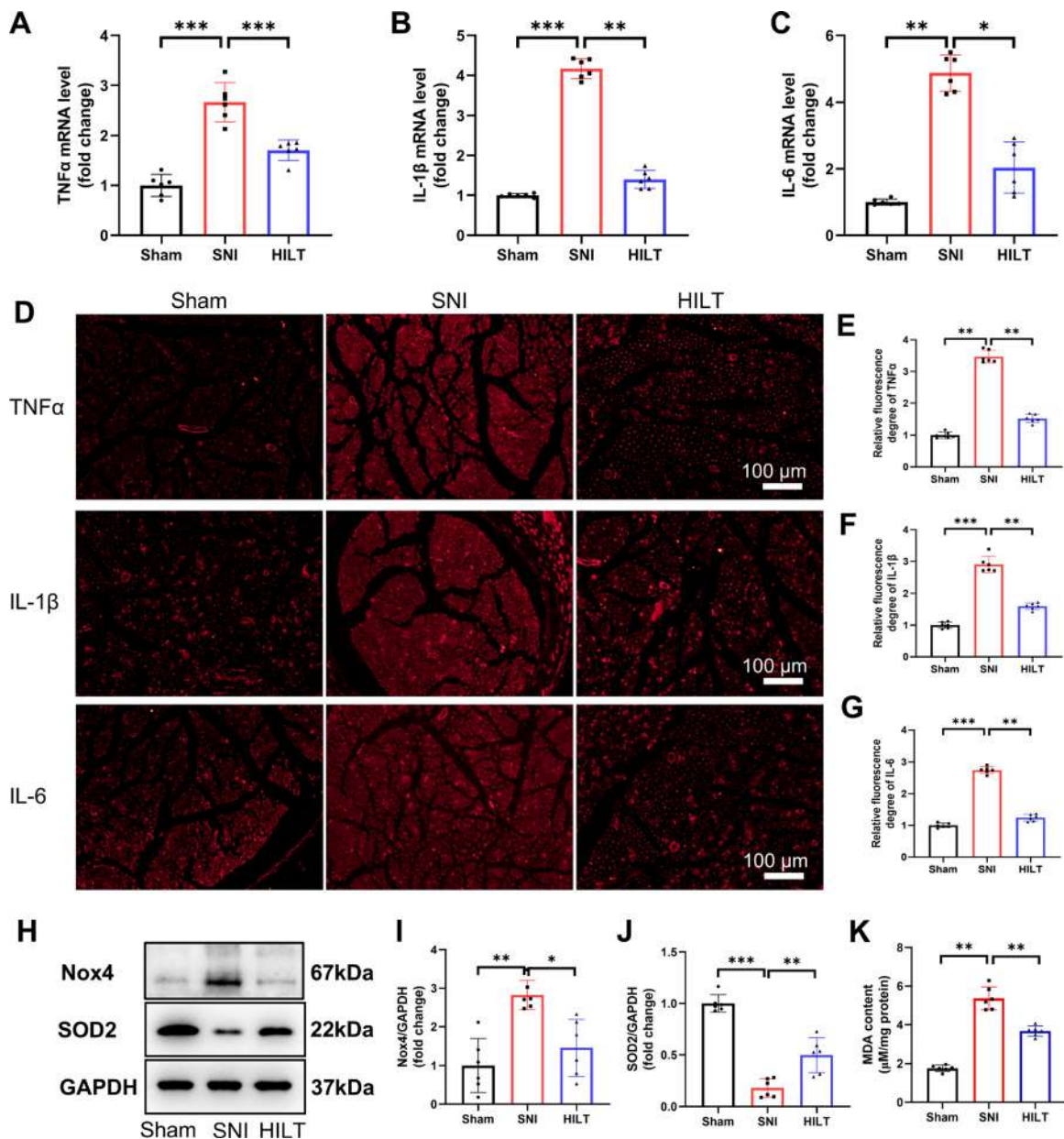


**FIG. 3.** HILT attenuates inflammation and oxidative stress after SNI. (a)–(c) Sciatic nerve tissue inflammatory factor mRNA expression was measured by RT-qPCR ( $n = 6$ ). (d) Immunofluorescence detection of inflammatory factor expression in the sciatic nerve. (e)–(g) Quantitative analysis of immunofluorescent regions by Image J. (h)–(j) Oxidative stress-related indicators (NOX4 and SOD2) in the sciatic nerve were detected by Western blotting. (k) The levels of MDA in rat sciatic nerves ( $n = 6$ ).  $^*p < 0.05$ ,  $^{**}p < 0.01$ , and  $^{***}p < 0.001$ . One-way ANOVA followed by Tukey's *post hoc* tests was performed to determine the  $p$  value in panels a–c, e–g, and i–k. Collectively, these results establish that HILT suppresses SNI-induced neuroinflammation and oxidative stress.

novel finding of our work is the elucidation of the BMP4-Smad9 pathway's role in HILT-mediated repair. Although this pathway has been implicated in inflammation and oxidative stress in other contexts,<sup>32,33</sup> its function in peripheral nerve regeneration has been largely unexplored. We discovered that SNI suppresses the BMP4-Smad9 pathway, whereas HILT treatment robustly reactivates it. The functional significance of this reactivation was confirmed by our loss-of-function and

gain-of-function experiments. The fact that the therapeutic efficacy of HILT was markedly reduced by the BMP-Smad inhibitor LDN193189 functionally links the activation of this pathway to HILT's pro-regenerative outcomes. Furthermore, Smad9 overexpression *in vitro* was sufficient to mimic the anti-inflammatory and antioxidant effects of HILT in SCs, providing compelling evidence for a cell-autonomous mechanism. This positions SCs as a primary cellular target through

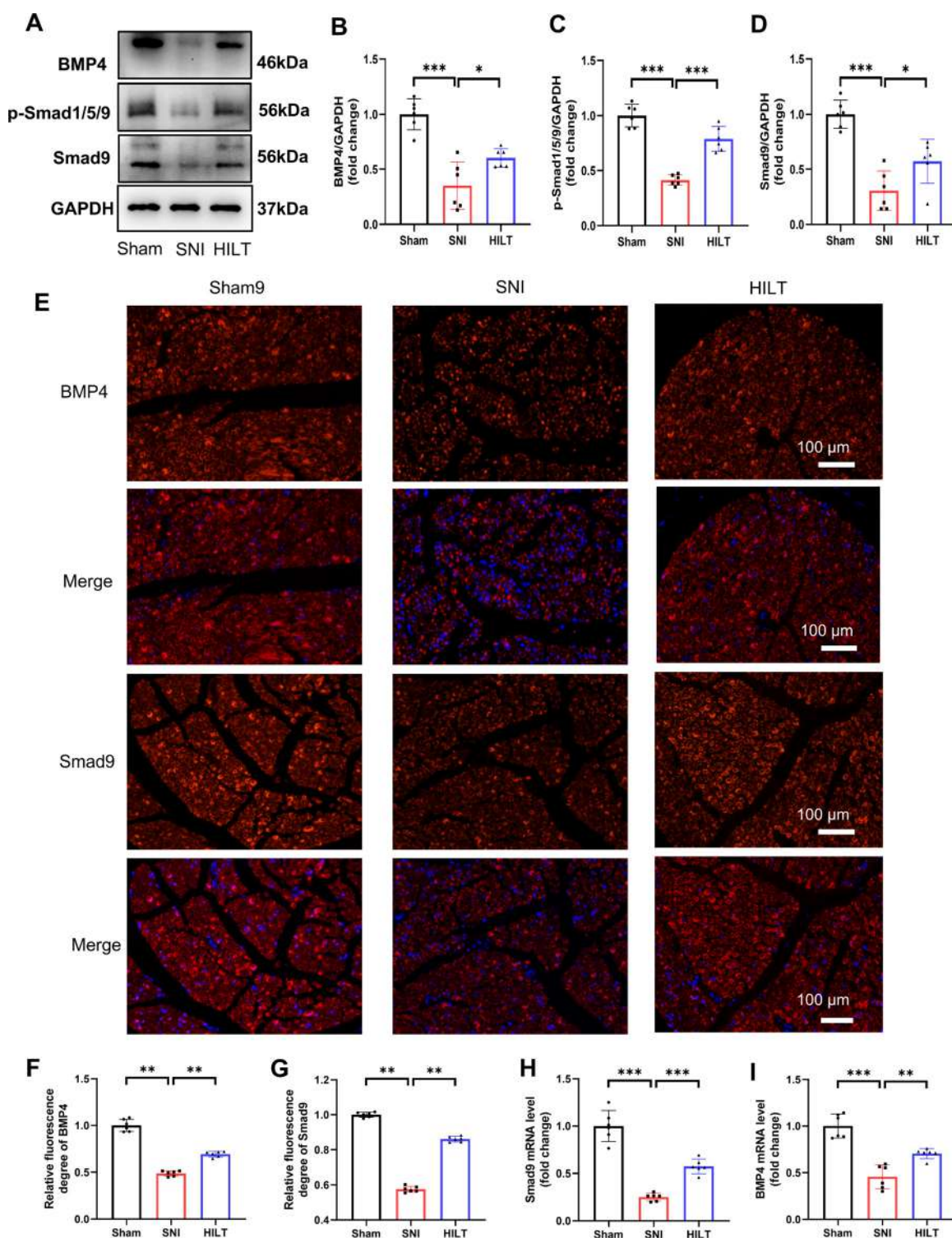


**FIG. 4.** HILT activates the BMP4-Smad9 signaling pathway in the sciatic nerve. (a)–(d) Western blot analysis of BMP4, p-Smad1/5/9, and Smad9 expression. (e) BMP4 and Smad9 immunofluorescence. Blue indicates nuclei stained with 4',6-diamidino-2-phenylindole (DAPI). Scale bar = 100 μm. (f) and (g) Analysis of BMP4 and Smad9 staining. (h) and (i) RT-qPCR for measuring mRNA expression of BMP4 and Smad9 in nerve tissues. \* $p < 0.05$ , \*\* $p < 0.01$ , \*\*\* $p < 0.001$ . One-way ANOVA followed by Tukey's *post hoc* tests was performed to determine the  $p$  value in panels b–d, and f–i. These data suggest that HILT activates the BMP4-Smad9 pathway, implicating it in the therapeutic response.

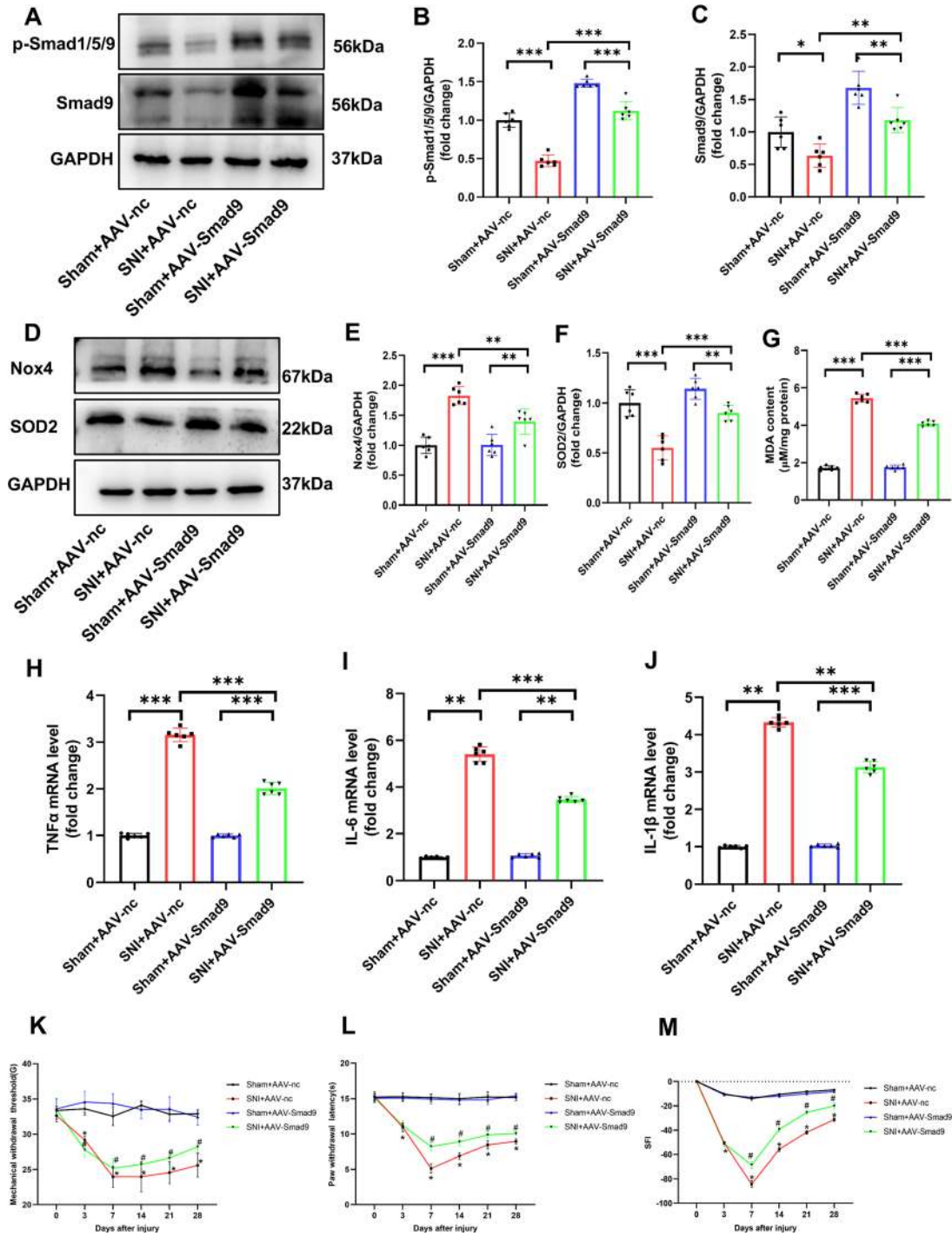


**FIG. 5.** Overexpression of Smad9 inhibits inflammation and oxidative stress and promotes neural repair. The AAV-Smad9 virus was injected into the sciatic nerve. (a)–(c) The expression level of p-Smad1/5/9 and Smad9 proteins was detected by Western blotting. (d)–(f) Protein expression of NOX4 and SOD2 was examined by Western blot analysis in nerve tissues. (g) The level of MDA was detected by the kit. (h)–(j) The mRNA levels of TNF- $\alpha$ , IL-1 $\beta$ , and IL-6 were determined by qRT-PCR. (k)–(l) The PWMT and PWL of each group were detected at 0, 3, 7, 14, 21, and 28 days (\* $p < 0.05$  vs Sham+ AAV-nc group; # $p < 0.05$  vs SNI+ AAV-nc group). (m) The functional recovery status was assessed using the SFI. \* $p < 0.05$ , \*\* $p < 0.01$ , \*\*\* $p < 0.001$ , and  $n = 6$  in each group. One-way ANOVA followed by Tukey's *post hoc* tests to determine the  $p$  value in panels b, c, and e–j, and repeated measurements ANOVA, followed by Tukey's *post hoc* tests to determine the  $p$  value in panels k–m. This demonstrates that Smad9 overexpression mitigates pathology and facilitates recovery, replicating HILT's benefits.

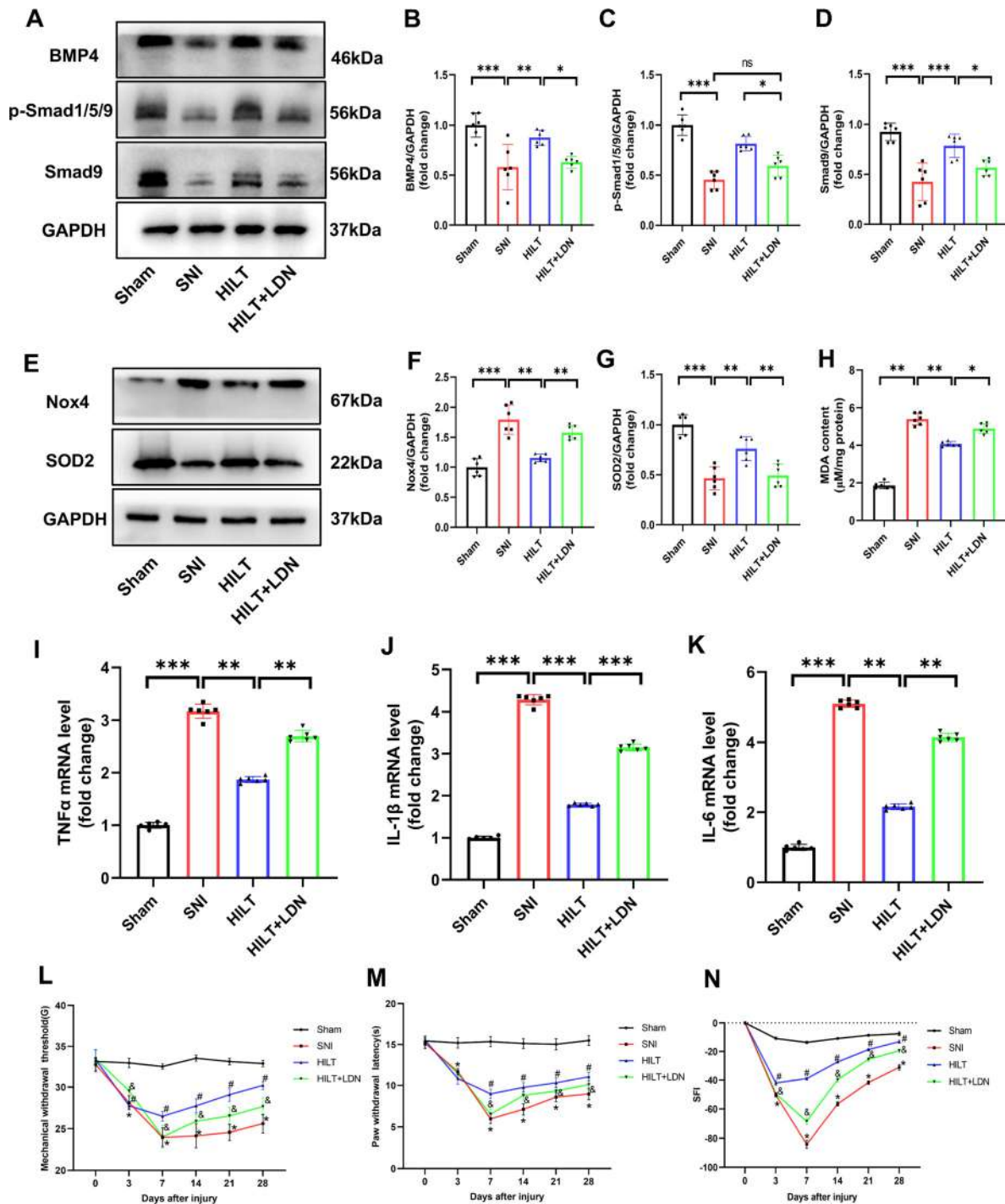


**FIG. 6.** The small molecule inhibitor LDN193189 reduces the therapeutic effect of HILT on SNI and exacerbates inflammation and oxidative stress. (a)–(d) Western blotting was used to find the corresponding protein expression. (e) Western blot analysis of NOX4 and SOD2 expression in the sham, SNI, HILT and HILT+ LDN groups. (f) and (g) Quantitative assessment of the expression of proteins linked to oxidative stress from (d). (h) Measurement of oxidative stress-related marker level (MDA). (i)–(k) The mRNA expressions of inflammatory factors were analyzed by RT-qPCR. (l)–(n) PWMT, PWL, and SFI were evaluated on 0, 3, 7, 14, 21, and 28 days (\**p* < 0.05 vs Sham group, #*p* < 0.05 vs SNI group, &*p* < 0.05 vs HILT group). The dose of LDN193189 (LDN) was 2 mg/kg. N = 6 rats/group. \**p* < 0.05, \*\**p* < 0.01, \*\*\**p* < 0.001, and n = 6 in each group. One-way ANOVA followed by Tukey’s *post hoc* tests to determine the *p* value in panels b–d and f–k, and repeated measurements ANOVA, followed by Tukey’s *post hoc* tests to determine the *p* value in panels l–n. Crucially, BMP-Smad pathway inhibition reverses HILT’s benefits, establishing its necessity for HILT-mediated recovery.

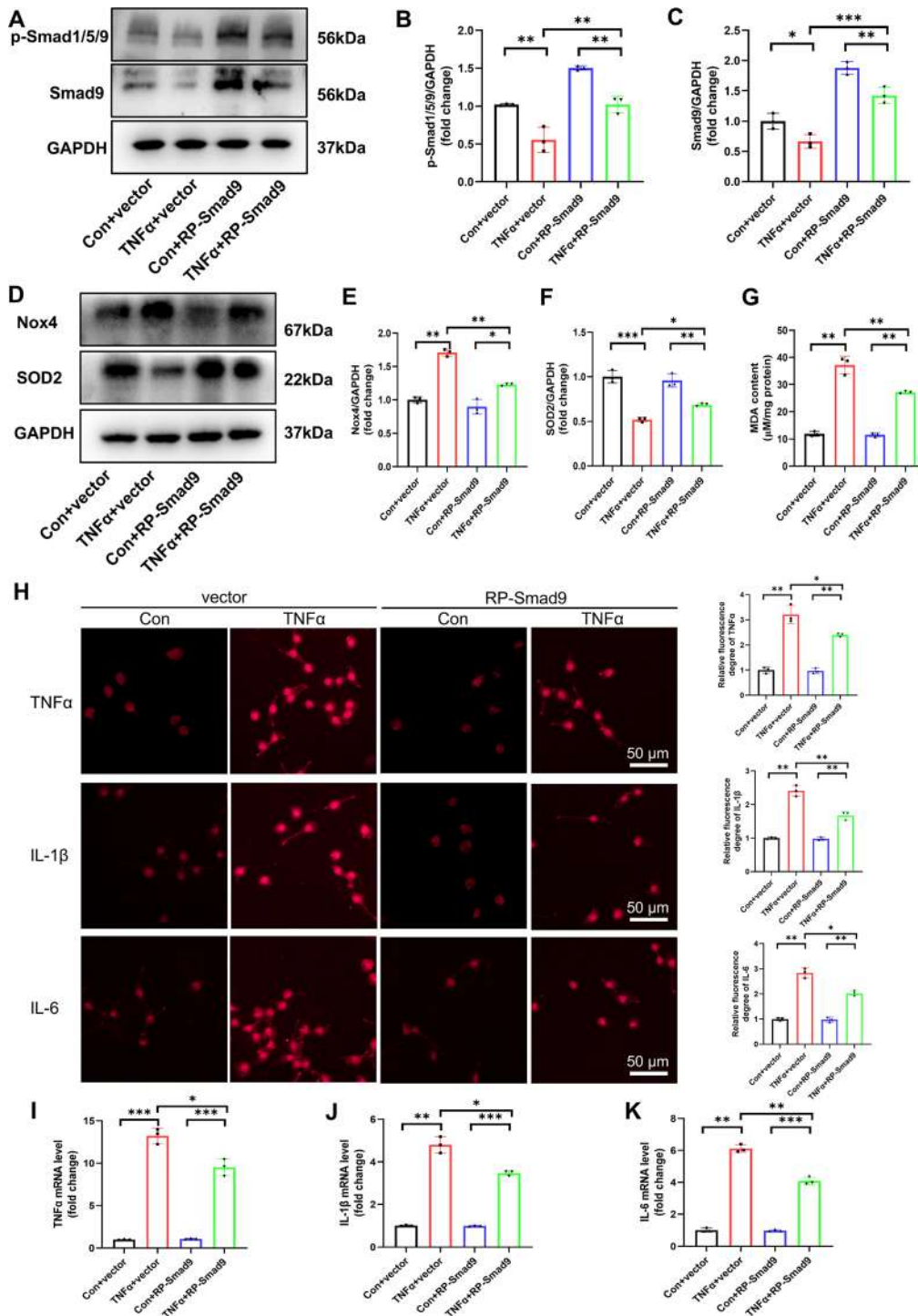


**FIG. 7.** Overexpression of Smad9 inhibits TNF- $\alpha$ -induced oxidative stress and inflammatory responses in SCs. (a)–(c) The protein expression level of p-Smad1/5/9 and Smad9 was analyzed by Western blotting. (d)–(f) The expression of oxidative stress proteins NOX4 and SOD2 was detected by Western blotting. (g) The activity of MDA was detected. (h) The expression of inflammatory factors (TNF- $\alpha$ , IL-1 $\beta$ , and IL-6) was assayed by immunofluorescence analyses. (i)–(k) The expression levels of inflammatory factor mRNA expression were measured by RT-qPCR. Three separate experiments were carried out. \* $p < 0.05$ , \*\* $p < 0.01$ , and \*\*\* $p < 0.001$ . One-way ANOVA followed by Tukey's *post hoc* tests was performed to determine the  $p$  value in panels b, c, and e–k. These *in vitro* findings provide mechanistic insight, showing that Smad9 activation within Schwann cells directly confers protection against inflammatory and oxidative insults, identifying a cell-autonomous mechanism for HILT's action.

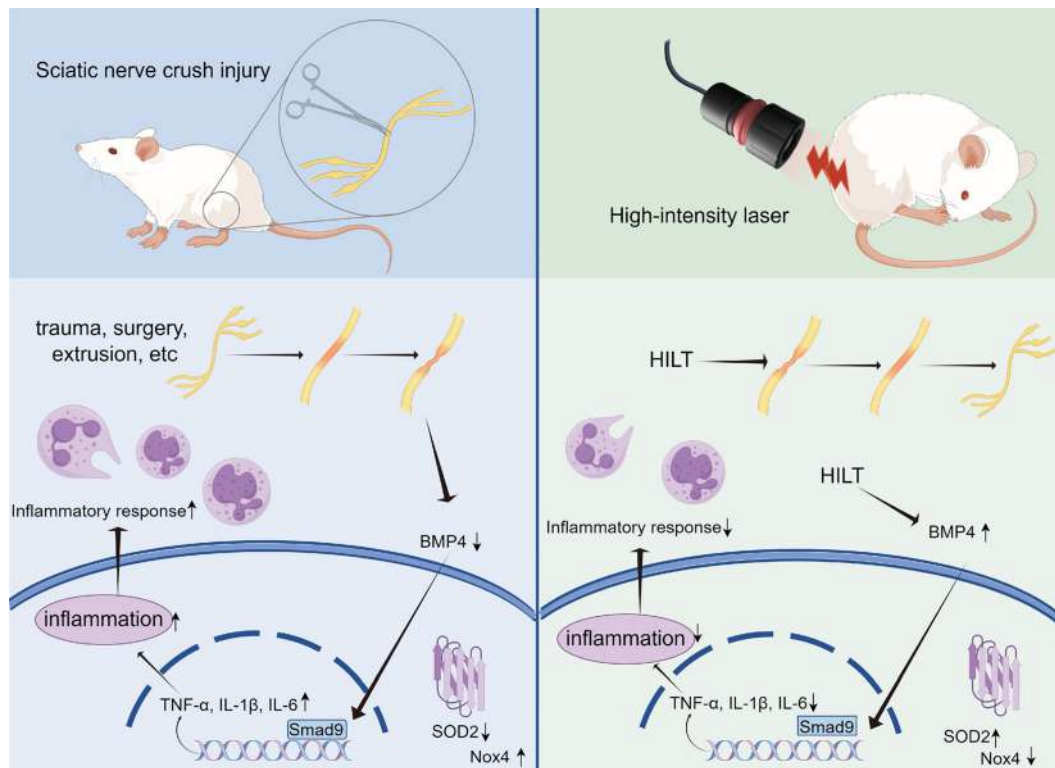


**FIG. 8.** HILT inhibits neuroinflammatory responses and oxidative stress through the BMP4-Smad9 pathway, thereby providing a potential means of alleviating sciatic nerve injury. HILT: high-intensity laser therapy; BMP4: Bone Morphogenetic Protein 4; Smad9: SMAD Family Member 9; SOD2: superoxide dismutase 2; NOX4: NADPH oxidase 4; TNF- $\alpha$ : tumor necrosis factor alpha; IL-1 $\beta$ : Interleukin-1beta; and IL-6: Interleukin-6.

which HILT, via BMP4-Smad9 signaling, orchestrates a conducive microenvironment for nerve repair.

We focused on the pivotal role of SCs, the key glial cells in peripheral nerve regeneration.<sup>46–49</sup> The upregulation of S100 $\beta$  and GAP43 following HILT treatment indicates enhanced SC activation and axonal regeneration, which underpins the observed functional improvements. The *in vitro* experiments confirm that the BMP4-Smad9 pathway is functional within SCs, and its activation can directly suppress TNF- $\alpha$ -induced inflammatory and oxidative stress responses. This cell-autonomous effect positions SCs as a crucial leverage point for HILT's therapeutic action.

While we establish the BMP4-Smad9 pathway as critical, we acknowledge the involvement of other signaling pathways, such as PI3K/AKT and NF- $\kappa$ B.<sup>25,50,51</sup> Our study focused on BMP4-Smad9 due to its pronounced activation by HILT in our initial screens and its relatively unexplored role in PNI. It is plausible that BMP4-Smad9 acts upstream or in parallel to these pathways, potentially converging on shared downstream targets like oxidative stress enzymes or pro-inflammatory cytokines. Elucidating the precise crosstalk between these networks represents an exciting direction for future research.

This study has certain limitations. Our study employed a well-established PNI model. While this model is widely accepted for studying peripheral nerve regeneration and pain mechanisms, it is important to note that it mimics traumatic nerve injury rather than the nerve root compression. Thus, our findings offer insights into PNI, and their

direct applicability to radicular pain warrants further investigation. A further limitation of this study is the lack of direct temperature monitoring during irradiation, which precludes definitive exclusion of thermal contributions. The exploration of HILT parameters, such as a broader dose range or different irradiation times, was limited by the scope of this investigation. Furthermore, the findings from the RSC96 Schwann cell line require verification by additional cell lines. Most importantly, the laser parameters effective in rodents cannot be directly applied to human patients due to key anatomical differences. Establishing optimized HILT protocols for clinical use, therefore, represents an essential goal for subsequent research.

Overall, the current study demonstrates that HILT inhibits muscle atrophy and facilitates nerve repair and functional rehabilitation after SNI, especially at moderate doses of HILT. It is the first time we find that the mechanism underlying this occurrence is perhaps connected to HILT-mediated inhibition of oxidative stress and neuroinflammation through the BMP4-Smad9 pathway, which promotes the proliferation of SCs. Our findings offer a novel approach and potential therapeutic target for the treatment of peripheral nerve injuries.

## CONCLUSION

In summary, HILT, especially at moderate doses, effectively delays gastrocnemius muscle atrophy after denervation and enhances nerve function and regeneration after SNI in a rat model. These beneficial effects are associated with the activation of the BMP4-Smad9

pathway and proliferation of SCs. Our findings suggest that the BMP4-Smad9 pathway may represent a potential mechanistic target for further investigation in the context of PNI, laying a foundation for future studies aimed at bridging regenerative biology with rehabilitation medicine.

## METHODS

### Materials

Recombinant rat TNF- $\alpha$  (TNF- $\alpha$ ) protein was obtained from R&D systems and dissolved in sterile phosphate buffer saline (PBS). LDN193189 (a selective inhibitor of the BMP signaling pathway, LDN) was acquired from Beyotime (Cat. No. SF7912). cDNA recombinant plasmid encoding Smad9 protein and the vector plasmid were acquired from GenePharma.

### Animals and modeling

Adult male Wistar rats (180–200 g) were procured from the Vital River Laboratories (Beijing, China) and raised in the Model Animal Center of Shandong University. Rats were raised at  $23 \pm 2^\circ\text{C}$  under a 12 h light/dark cycle with *ad libitum* access to a standard diet and water. Three rats per cage were housed following established protocols to ensure welfare and minimize distress during experimentation. Following a week of adaptive feeding, a model of sciatic nerve injury was successfully established. To minimize procedural variability, all surgical interventions were performed by a single operator on the same day. The sample size of  $n = 6$  per group was determined based on a power analysis conducted using preliminary data, which indicated this number was sufficient to detect significant differences in the primary outcome measures. In our study, the animals were randomly assigned to different experimental groups using a computer-generated random number table. Specifically, after the completion of all surgical procedures, each animal was given a unique identification number, and then these numbers were randomly shuffled using a random number generator. The animals were then assigned to the different groups based on the order of the shuffled numbers. The group allocation list was concealed from the investigators performing the subsequent behavioral assessments and data analysis. This method ensures that each animal has an equal chance of being assigned to any of the experimental groups ( $n = 6$  per group), thus minimizing the potential for bias. At the experimental end point, all rats were anesthetized via intraperitoneal administration of sodium pentobarbital (50 mg/kg). The efficacy of anesthesia was confirmed by the absence of a toe-pinch withdrawal reflex. The animals were then humanely euthanized by exsanguination under deep anesthesia.<sup>52</sup> All experimental procedures were conducted in strict adherence to the “3R principles” (replacement, reduction, and refinement), with the number of rats used in each experiment being statistically maintained at the minimum possible number. All efforts were made to reduce the number of animals used and to minimize their suffering. All experimental protocols were examined and approved by the Animal Ethical and Welfare Committee of Shandong University (Approval No. 23055).

The rats were anesthetized with sodium pentobarbital (50 mg/kg of body weight, via intraperitoneal injection) and shaved on their rear limbs and lower back and cleaned with iodine. Rat eyes were treated with an ophthalmic solution to avoid drying out. A skin cut was made, and a blunt separation was used to access the biceps femoris. Subsequently, a sciatic nerve crush injury model of around 2 mm was

induced by clamping the sciatic nerve trunk thrice with toothless hemostatic forceps (Fine Science Tools, Germany) for 10 s each time, at an interval of 10 s. Although the Sham group's sciatic nerve was exposed, there was no crush damage. A successful SNI model was characterized by a significant left hind paw fall, with deep bending and inversion of the toes. To ensure consistency of the SNI model, the sciatic nerve was exposed via a defined posterior thigh incision, and injury was induced at a consistent anatomical location. Preoperative and postoperative animal weight, activity levels, and wound healing were monitored daily to ensure uniformity in postoperative recovery conditions.

### HILT treatment

Irradiation was performed using a pulsed Nd:YAG laser (HERO-3 laser, ASA, Arcugnano, Vicenza, Italy). The laser system had the following specifications: a wavelength of 1064 nm, a pulse duration of 100  $\mu\text{s}$ , a peak power of 3000 W, a beam diameter of 0.5 cm (beam area: 0.2  $\text{cm}^2$ ), and a nominal average power of 10.5 W. The laser probe was positioned perpendicularly and 1 cm from the skin surface, avoiding contact with the injured area. To achieve uniform irradiation over the tissue surrounding the sciatic nerve injury site (approximately 10  $\text{cm}^2$ ), laser irradiation was applied using a standardized scanning protocol, consistent with engineering assumptions and prior literature. The laser was operated at a pulse repetition rate of 10 Hz. At the single spot level, the fluence per pulse was maintained at 360  $\text{mJ}/\text{cm}^2$ , corresponding to an energy per pulse of approximately 70 mJ. These parameters were held constant across all treatment conditions. Under the applied experimental settings, the time-averaged delivered power was approximately 0.7 W. The nominal average power of 10.5 W refers to the manufacturer-rated maximum system capability and was not the power delivered in the experiments. The different total energy densities administered to the treatment groups (HILT-10, HILT-50, and HILT-100) were achieved by varying the scan duration (Table II). The HILT-10, HILT-50, and HILT-100 groups received total energies of 100, 500, and 1000 J, respectively, over the 10  $\text{cm}^2$  area, with corresponding treatment durations of 2.4, 12, and 24 min. Accordingly, the HILT-10, HILT-50, and HILT-100 groups received cumulative fluences of approximately 10, 50, and 100  $\text{J}/\text{cm}^2$ , respectively, over the 10  $\text{cm}^2$  treatment area. Dose differentiation among treatment groups was achieved exclusively by varying the irradiation duration, while all other laser parameters remained unchanged. The laser treatment was applied 5 days a week for 4 weeks. The laser parameters were calculated following the method described in the prior literature.<sup>42</sup>

Manufacturer-rated nominal average power represents the maximum system specification and was not used for experimental dosimetry calculations.

### Walking track analysis

Sciatic function indexes (SFIs) of the rats were measured before damage and on days 3, 7, 14, 21, and 28 after injury using a walking track analysis. Briefly, the plantar surface of the rat's hind paws was coated with black ink. All rats were guided along a straight course on a white paper. Then clear footprints were considered and SFI was calculated. SFI values ranged between 0 and  $-100$ , with  $-100$  indicating that all nerves had been destroyed. To ensure objectivity, all footprint measurements and SFI calculations were performed by two

**TABLE II.** Laser system specifications and experimentally applied dosimetry parameters.

Category	Parameter	Value
Laser system (manufacturer specification)	Wavelength	1064 nm
	Pulse width	100 $\mu$ s
	Maximum power	3000 W
	Nominal average power	10.5 W
	Beam diameter	0.5 cm
	Beam area	0.2 cm <sup>2</sup>
Fixed experimental parameters	Frequency	10 Hz
	Fluence per pulse (at beam area)	360 mJ/cm <sup>2</sup>
Dose-controlled parameters	Irradiation duration	(HILT-10) 2.4 min
		(HILT-50) 12 min
		(HILT-100) 24 min
Delivered dose (treatment area)	Cumulative fluence (treatment area)	(HILT-10) 10 J/cm <sup>2</sup>
		(HILT-50) 50 J/cm <sup>2</sup>
		(HILT-100) 100 J/cm <sup>2</sup>

experienced researchers who were blinded to the group allocation of the animals.

### Nociceptive behavior

Behavioral assessments of the ipsilateral hind paw were performed preoperatively and on postoperative days 3, 7, 14, 21, and 28. For mechanical hyperalgesia evaluation, rats were acclimated in transparent plexiglass chambers with metal mesh floors for 30 min. Paw withdrawal mechanical threshold (PWMT) was measured using von Frey filaments ((kw-CT-1, Calvin biotechnology, Nanjing, China) applied perpendicularly to the plantar surface of the left hind paw. A positive response was defined as rapid paw withdrawal or licking.

Thermal hyperalgesia was assessed using a radiant heat stimulator (KW600 Calvin Biotechnology, Nanjing, China). Rats were placed in glass chambers and allowed 30 min for acclimation. The paw withdrawal latency (PWL) was recorded as the interval between heat application to the hind paw plantar surface and observable withdrawal/licking responses. A 20-s automatic cutoff prevented tissue damage. Three trials were conducted at 5-min intervals, with mean scores used for statistical analysis. For all behavioral tests, the investigators performing the assessments were different from the surgeon and were fully blinded to the experimental group assignment throughout the data collection and initial analysis process.

### Cell culture and treatments

The Chinese Academy of Sciences' Cell Bank in Shanghai, China, provided the rat SC line RSC96, which was cultivated in Minimum Essential Medium (MEM) supplemented with 10% endotoxin-free fetal calf serum. Reagent administration was carried out after cells reached 70%–80% confluence. To determine the optimal time point for the administration of this agent, SCs were first stimulated with tumor necrosis factor- $\alpha$  (TNF- $\alpha$ , 10 ng/ml) for 0, 1, 3, 6, 12, and 24 h. After analysis, it was found that the ideal time point was 3 h. In *in vitro* tests, SCs were preincubated with TNF- $\alpha$  for 3 h. All cell-based experiments were performed in three independent biological replicates.

### Real-time quantitative PCR (RT-qPCR)

RNA was extracted using commercially available RNA extraction kits (Fastagen Biotech, Shanghai) and reverse transcribed into complementary DNA (cDNA) using an RT-PCR kit. The RT-qPCR procedure was carried out in accordance with the manufacturer's instructions (GeneCopoeia). The primer sequences utilized are detailed in the [supplementary material](#).

### Western blotting

Cultured cells and sciatic nerve tissues were homogenized with radioimmunoprecipitation assay (RIPA) lysis buffer (Beyotime Biotechnology). Protein samples were separated on sodium dodecyl-sulfate polyacrylamide gel electrophoresis (SDS-PAGE) and transferred to polyvinylidene difluoride membranes. Membranes were blocked with skim milk (5% in phosphate buffer saline with Tween-20 (PBST)) at room temperature for 1 h, after which they were incubated at 4 °C overnight with primary antibodies, including anti-BMP4 (1:1000, Cat# 12492-1-AP, Proteintech), anti-p-Smad1/5/9 (1:1000, Cat# HA722566, HuaBio), anti-Smad9 (1:1000, Cat# AF5114, Affinity), anti-growth-associated protein 43 (GAP43) (1:1000, Cat# ab75810, Abcam), anti-S100 calcium-binding protein beta (S100 $\beta$ ) (1:1000, Cat# ab52642, Abcam), or anti-glyceraldehyde 3-phosphate dehydrogenase (GAPDH) (1:1000, Cat# AB-P-R001, Good Here). Following treatment with a secondary antibody coupled with horseradish peroxidase, blots were created in enhanced chemiluminescent (ECL) substrates (BOSTER). An ECL method (Millipore) was used to visualize the blots. Image J software (NIH, Bethesda, MD, USA) was used for the densitometric analysis.

### Histological assessment

For hematoxylin and eosin (H&E) staining, after dehydration with a range of graded alcohols, sciatic nerve tissues were fixed in 4% paraformaldehyde (PFA). The specimen was embedded in a paraffin block following xylene treatment and then sliced at a thickness of 5  $\mu$ m. After that, sections were stained using H&E in accordance with

established protocols. For immunofluorescence staining, after 30 min of room temperature preservation in 4% PFA, tissue sections or cell cultures were subjected to 15 min of 0.1% Triton X-100 treatment and 30 min of 5% bovine serum albumin treatment. Afterward, cell or tissue samples were incubated at 4 °C for a period of 12–16 h with primary antibodies, including anti-GAP43 (1:200, Cat# ab75810, Abcam), anti-S100 $\beta$  (1:200, Cat# ab52642, Abcam), anti-TNF- $\alpha$  (1:300, Cat# ab6671, Abcam), anti-IL-1 $\beta$  (1:200, Cat# ET1701-39, Huabio), anti-IL-6 (1:200, Cat# R1412-2, Huabio), anti-Smad9 (1:200, Cat# ER64980, Huabio), and anti-BMP4 (1:200, Cat# 12492-1-AP, Proteintech), followed by incubation with a fluorescence-conjugated secondary antibody (1:200, Abbkine). Samples were then labeled with DAPI (Cat# ab104139, Abcam) for 10 min. Using a Nikon fluorescent microscope, samples were examined. For toluidine blue staining and electron microscopy, the regenerated nerves were fixed in 2.5% glutaraldehyde at 4 °C for 48 h, followed by post-fixing with 1% osmium tetroxide, ethanol dehydration, and embedding in Epon812 resin. Then 1  $\mu$ m thick sections were taken from each sample and stained with 1% toluidine blue for light microscopy observation. Additionally, 50 nm thick sections were stained with lead citrate and uranyl acetate, followed by examination under a transmission electron microscope (TEM, HT7700, Hitachi, Japan). The Image J software was used to calculate the fluorescence intensity, the diameter and density of myelinated nerve fibers, the area of the myelinated axons, and myelin sheath thickness. Furthermore, the G-ratio, defined as axon diameter divided by large fiber diameter of the myelin sheath, was also calculated. The images were analyzed by a trained evaluator blinded to group assignment.

### Statistical analysis

The mean  $\pm$  standard deviation (SD) was used to express all data. GraphPad Prism 8 (GraphPad Software, Inc., San Diego, CA) was employed for graph generation and data analysis. One-way analysis of variance (ANOVA) followed by Tukey's *post hoc* test was utilized to assess the statistical differences among multiple groups, except for behavioral measurement data, which were analyzed using repeated measures ANOVA.  $P < 0.05$  was used as the threshold for statistical significance.

### SUPPLEMENTARY MATERIAL

See the [supplementary material](#) for primers for RT-qPCR experiments, as well as a supporting figure that further validates the findings presented in the main text.

### ACKNOWLEDGMENTS

This study was funded by the Natural Science Foundation of China under Grant Nos. 82372564 and 82172535, the Introduce Innovative Teams of 2021 New High School 20 Items Project under Grant No. 2021GXRC098, and the Natural Science Foundation of Shandong Province under Grant No. ZR2022QH022.

### AUTHOR DECLARATIONS

#### Conflict of Interest

The authors have no conflicts to disclose.

### Ethics Approval

Ethics approval for experiments reported in the submitted manuscript on animal or human subjects was granted. All methods and procedures described below were pre-approved by the Animal Ethical and Welfare Committee of Shandong University (Approval No. 23055). The study was conducted in accordance with the local legislation and institutional requirements.

### Author Contributions

**Lanlan Gong:** Conceptualization (equal); Validation (equal); Writing – original draft (equal). **Danyang Li:** Funding acquisition (equal); Investigation (equal). **Xiaojing Zhao:** Formal analysis (equal). **Yujuan Qu:** Formal analysis (equal). **Shasha Song:** Methodology (equal); Resources (equal). **Jialin Liu:** Methodology (equal). **Shouwei Yue:** Conceptualization (equal); Funding acquisition (equal); Supervision (equal).

### DATA AVAILABILITY

The data that support the findings of this study are available from the corresponding author upon reasonable request.

### REFERENCES

- <sup>1</sup>B. Lopes, P. Sousa, R. Alvites, M. Branquinho, A. C. Sousa, C. Mendonça *et al.*, “Peripheral nerve injury treatments and advances: One health perspective,” *Int. J. Mol. Sci.* **23**(2), 918 (2022).
- <sup>2</sup>T. Li, G. Lin, T. Zhang, Y. Guo, Y. He, J. Luan *et al.*, “Repetitive transcranial magnetic stimulation ameliorates chronic pain behavior and modulates the brain transcriptome in a mouse model of chronic constriction injury,” *Brain Res. Bull.* **227**, 111383 (2025).
- <sup>3</sup>S. H. Chen, H. K. Kao, J. R. Wun, P. Y. Chou, Z. Y. Chen, S. H. Chen *et al.*, “Thermosensitive hydrogel carrying extracellular vesicles from adipose-derived stem cells promotes peripheral nerve regeneration after microsurgical repair,” *APL Bioeng.* **6**(4), 046103 (2022).
- <sup>4</sup>L. Cao, W.-H. Yan, W. Pi, Y. Zhang, Y.-X. Xiong, V. W. Yong *et al.*, “GABAB receptors regulate the neural stem cell potential of Pkd211+ cerebrospinal fluid-contacting neurons via the PI3K/Akt signaling pathway,” *Brain Res. Bull.* **221**, 111217 (2025).
- <sup>5</sup>L. Mathieu, Y. Cloquell, J. C. Murison, G. Pfister, C. Gaillard, C. Oberlin *et al.*, “Defects of the sciatic nerve and its divisions treated by direct suturing in 90 degrees knee flexion: Report on the first clinical series,” *Eur. J. Trauma Emerg. Surg.* **48**(6), 4955–4962 (2022).
- <sup>6</sup>L.-P. Cen, T. K. Ng, J.-J. Liang, C. Xu, X. Zhuang, Y.-F. Liu *et al.*, “Agonist of growth hormone-releasing hormone enhances retinal ganglion cell protection induced by macrophages after optic nerve injury,” *Proc. Natl. Acad. Sci. U. S. A.* **118**(28), e1920834118 (2021).
- <sup>7</sup>R. Li, D. Li, C. Wu, L. Ye, Y. Wu, Y. Yuan *et al.*, “Nerve growth factor activates autophagy in Schwann cells to enhance myelin debris clearance and to expedite nerve regeneration,” *Theranostics* **10**(4), 1649–1677 (2020).
- <sup>8</sup>R.-C. Zhang, W.-Q. Du, J.-Y. Zhang, S.-X. Yu, F.-Z. Lu, H.-M. Ding *et al.*, “Mesenchymal stem cell treatment for peripheral nerve injury: A narrative review,” *Neural Regen. Res.* **16**(11), 2170–2176 (2021).
- <sup>9</sup>X. Zeng, W. Bian, Z. Liu, J. Li, S. Ren, J. Zhang *et al.*, “Muscle-derived stem cell exosomes with overexpressed miR-214 promote the regeneration and repair of rat sciatic nerve after crush injury to activate the JAK2/STAT3 pathway by targeting PTEN,” *Front. Mol. Neurosci.* **16**, 1146329 (2023).
- <sup>10</sup>R. A. Suhar, L. M. Marquardt, S. Song, H. Buabbas, V. M. Doulames, P. K. Johansson *et al.*, “Elastin-like proteins to support peripheral nerve regeneration in guidance conduits,” *ACS Biomater. Sci. Eng.* **7**(9), 4209–4220 (2021).
- <sup>11</sup>X.-L. Chu, X.-Z. Song, Q. Li, Y.-R. Li, F. He, X.-S. Gu *et al.*, “Basic mechanisms of peripheral nerve injury and treatment via electrical stimulation,” *Neural Regen. Res.* **17**(10), 2185–2193 (2022).

- <sup>12</sup>S. Iwabuchi, Y. Hara, Y. Yoshii, and M. Yamazaki, "A favourable suture method for size-mismatched nerve transfer: A case series of intercostal-to-musculocutaneous nerve transfer for brachial plexus injury," *J. Hand Surg.* **49**(2), 267–269 (2024).
- <sup>13</sup>L. Cao, Z. Shanguan, Y. Zhang, Z. Luo, C. Chen, H. Yan *et al.*, "Vegfr3 activation of Pkd2l1+ CSF-cNs triggers the neural stem cell response in spinal cord injury," *Cell Signal* **130**, 111675 (2025).
- <sup>14</sup>E. Tunç, E. S. Bora, and O. Erbaş, "Harnessing polyethylene glycol 3350 for enhanced peripheral nerve repair: A path to accelerated recovery," *Medicina* **61**(4), 624 (2025).
- <sup>15</sup>G. Nocera and C. Jacob, "Mechanisms of Schwann cell plasticity involved in peripheral nerve repair after injury," *Cell. Mol. Life Sci.* **77**(20), 3977–3989 (2020).
- <sup>16</sup>J. C. Lee, S. W. P. Kemp, and T. A. Kung, "Regenerative peripheral nerve interface surgery for the management of chronic posttraumatic neuropathic pain," *Semin. Plast. Surg.* **38**(1), 19–24 (2024).
- <sup>17</sup>M. A. Ahmad, M. S. A. Hamid, and A. Yusof, "Effects of low-level and high-intensity laser therapy as adjunctive to rehabilitation exercise on pain, stiffness and function in knee osteoarthritis: A systematic review and meta-analysis," *Physiotherapy* **114**, 85–95 (2022).
- <sup>18</sup>Y. Huang and D. Gao, "The effectiveness of high intensity laser therapy in the patients with lumbar disc herniation: A protocol of randomized placebo-controlled trial," *Medicine* **99**(41), e22520 (2020).
- <sup>19</sup>M. S. M. Alayat, T. H. A. Aly, A. E. M. Elsayed, and A. S. M. Fadil, "Efficacy of pulsed Nd:YAG laser in the treatment of patients with knee osteoarthritis: A randomized controlled trial," *Lasers Med. Sci.* **32**(3), 503–511 (2017).
- <sup>20</sup>M. A. Ahmad, M. Moganan, M. S. A. Hamid, N. Sulaiman, U. Moorthy, N. Hasnan *et al.*, "Comparison between low-level and high-intensity laser therapy as an adjunctive treatment for knee osteoarthritis: A randomized, double-blind clinical trial," *Life* **13**(7), 1519 (2023).
- <sup>21</sup>S. B. Sen, M. Kosehasanogullari, N. O. Yilmaz, and B. F. Kocuyigit, "Comparative analysis of the therapeutic effects of extracorporeal shock wave therapy and high-intensity laser therapy in lateral epicondylitis: A randomised clinical trial," *Rheumatol. Int.* **44**(4), 593–602 (2024).
- <sup>22</sup>C. Yu, X. Wang, and J. Qin, "Effect of necrostatin-1 on sciatic nerve crush injury in rat models," *J. Orthop. Surg. Res.* **18**(1), 74 (2023).
- <sup>23</sup>K. Molnár, B. Nógrádi, R. Kristóf, Á. Mészáros, K. Pajer, L. Siklós *et al.*, "Motoneuronal inflammasome activation triggers excessive neuroinflammation and impedes regeneration after sciatic nerve injury," *J. Neuroinflammation* **19**(1), 68 (2022).
- <sup>24</sup>X. Bai, G. Batallé, I. Martínez-Martel, and O. Pol, "Hydrogen sulfide interacting with cannabinoid 2 receptors during sciatic nerve injury-induced neuropathic pain," *Antioxidants* **12**(6), 1179 (2023).
- <sup>25</sup>J. Wei, W. Su, Y. Zhao, Z. Wei, Y. Hua, P. Xue *et al.*, "Maresin 1 promotes nerve regeneration and alleviates neuropathic pain after nerve injury," *J. Neuroinflammation* **19**(1), 32 (2022).
- <sup>26</sup>O. Avraham, R. Feng, E. E. Ewan, J. Rustenhoven, G. Zhao, and V. Cavalli, "Profiling sensory neuron microenvironment after peripheral and central axon injury reveals key pathways for neural repair," *Elife* **10**, e68457 (2021).
- <sup>27</sup>T.-C. Huang, H.-L. Wu, S.-H. Chen, Y.-T. Wang, and C.-C. Wu, "Thrombomodulin facilitates peripheral nerve regeneration through regulating M1/M2 switching," *J. Neuroinflammation* **17**(1), 240 (2020).
- <sup>28</sup>S. A. Khodir, S. Imbaby, M. S. Abdel Allem Amer, M. M. Atwa, F. A. Ashour, and A. A. Elbaz, "Effect of mesenchymal stem cells and melatonin on experimentally induced peripheral nerve injury in rats," *Biomed. Pharmacother.* **177**, 117015 (2024).
- <sup>29</sup>M. Haddad, S. Eid, F. Harb, M. E. L. Massry, S. Azar, E.-A. Sauleau *et al.*, "Activation of 20-HETE synthase triggers oxidative injury and peripheral nerve damage in type 2 diabetic mice," *J. Pain* **23**(8), 1371–1388 (2022).
- <sup>30</sup>A. Razaq, G. Hussain, A. Rasul, J. Xu, Q. Zhang, S. A. Malik *et al.*, "Strychnos nux-vomica L. seed preparation promotes functional recovery and attenuates oxidative stress in a mouse model of sciatic nerve crush injury," *BMC Complementary Med. Ther.* **20**(1), 181 (2020).
- <sup>31</sup>R. Xue, M. Xie, Z. Wu, S. Wang, Y. Zhang, Z. Han *et al.*, "Mesenchymal stem cell-derived exosomes promote recovery of the facial nerve injury through regulating macrophage M1 and M2 polarization by targeting the P38 MAPK/NF- $\kappa$ B pathway," *Aging Dis.* **15**(2), 851–868 (2024).
- <sup>32</sup>Z. Zhang, X. Zhao, M. Gao, L. Xu, Y. Qi, J. Wang *et al.*, "Dioscin alleviates myocardial infarction injury via regulating BMP4/NOX1-mediated oxidative stress and inflammation," *Phytomedicine* **103**, 154222 (2022).
- <sup>33</sup>T. Ahsan, S. S. Shoily, T. Ahmed, and A. A. Sajib, "Role of the redox state of the Pirin-bound cofactor on interaction with the master regulators of inflammation and other pathways," *PLoS One* **18**(11), e0289158 (2023).
- <sup>34</sup>C.-H. Tsai, E. Liu, A. Phan, K. L. Lu, and H. Mei, "NBL1 reduces corneal fibrosis and scar formation after wounding," *Biomolecules* **13**(11), 1570 (2023).
- <sup>35</sup>C. Chen, C. Song, B. Liu, Y. Wang, J. Jia, K. Pang *et al.*, "Activation of BMP4/SMAD pathway by HIF-1 $\alpha$  in hypoxic environment promotes osteogenic differentiation of BMSCs and leads to ectopic bone formation," *Tissue Cell* **88**, 102376 (2024).
- <sup>36</sup>F. Yiğit and B. Ordahan, "Effects of high-intensity laser therapy on pain, functional status, hand grip strength, and median nerve cross-sectional area by ultrasonography in patients with carpal tunnel syndrome," *Lasers Med. Sci.* **38**(1), 248 (2023).
- <sup>37</sup>P.-Y. Ko, C.-C. Hsu, S.-Y. Chen, C.-L. Li, I. M. Jou, and P.-T. Wu, "The pulsed Nd:YAG laser therapy enhanced nerve regeneration via apoptosis inhibition in a rat crushed sciatic nerve model," *Neurochem. Res.* **49**(4), 949–958 (2024).
- <sup>38</sup>T. Akgul, M. Gulsoy, and H. O. Gulcur, "Effects of early and delayed laser application on nerve regeneration," *Lasers Med. Sci.* **29**(1), 351–357 (2014).
- <sup>39</sup>C. Laotammateep, J. Champaiboon, T. Surarangsit, W. Likhithiphthak, and J. Boonhong, "Efficacy of high intensity laser therapy versus sham laser in symptomatic knee osteoarthritis: A double-blind randomized controlled trial," *Lasers Med. Sci.* **40**(1), 87 (2025).
- <sup>40</sup>U. Dundar, U. Turkmen, H. Toktas, O. Solak, and A. M. Ulasli, "Effect of high-intensity laser therapy in the management of myofascial pain syndrome of the trapezius: A double-blind, placebo-controlled study," *Lasers Med. Sci.* **30**(1), 325–332 (2015).
- <sup>41</sup>Y.-Y. Huang, S. K. Sharma, J. Carroll, and M. R. Hamblin, "Biphasic dose response in low level light therapy—An update," *Dose Response* **9**(4), 602–618 (2011).
- <sup>42</sup>M. S. M. Alayat, M. A. Basalamah, W.-E. Elbarrany, N. A. M. El-Sawy, E. M. Abdel-Kafy, and A. A.-R. El-Fiky, "Dose-dependent effect of the pulsed Nd:YAG laser in the treatment of crushed sciatic nerve in Wister rats: An experimental model," *Lasers Med. Sci.* **35**(9), 1989–1998 (2020).
- <sup>43</sup>S. Wu, Z. Jiang, J. Dong, and M. Yao, "Evaluation of thermodynamic bioeffects of long-pulsed 1064 nm laser in the photothermal lipolysis," *Lasers Surg. Med.* **56**(1), 90–99 (2024).
- <sup>44</sup>T. Gould, Q. Wang, and T. J. Pfefer, "Optical-thermal light-tissue interactions during photoacoustic breast imaging," *Biomed. Opt. Express* **5**(3), 832–847 (2014).
- <sup>45</sup>L. Wang, S. L. Jacques, and L. Zheng, "MCML—Monte Carlo modeling of light transport in multi-layered tissues," *Comput. Methods Programs Biomed.* **47**(2), 131–146 (1995).
- <sup>46</sup>M. Bosch-Queralt, R. Fledrich, and R. M. Stassart, "Schwann cell functions in peripheral nerve development and repair," *Neurobiol. Dis.* **176**, 105952 (2023).
- <sup>47</sup>A. Murtazina and I. Adameyko, "The peripheral nervous system," *Development* **150**(9), dev201164 (2023).
- <sup>48</sup>A.-L. Cattin, J. J. Burden, L. Van Emmenis, F. E. Mackenzie, J. J. A. Hoving, N. Garcia Calavia *et al.*, "Macrophage-induced blood vessels guide Schwann cell-mediated regeneration of peripheral nerves," *Cell* **162**(5), 1127–1139 (2015).
- <sup>49</sup>A. Fuentes-Flores, C. Geronimo-Olvera, K. Girardi, D. Necuñir-Ibarra, S. K. Patel, J. Bons *et al.*, "Senescent Schwann cells induced by aging and chronic denervation impair axonal regeneration following peripheral nerve injury," *EMBO Mol. Med.* **15**(12), e17907 (2023).
- <sup>50</sup>Y. Zhang, D. Yi, Q. Hong, J. Cao, X. Geng, J. Liu *et al.*, "Platelet-rich plasma-derived exosomes boost mesenchymal stem cells to promote peripheral nerve regeneration," *J. Controlled Release* **367**, 265–282 (2024).
- <sup>51</sup>Q. Yang, S. Su, S. Liu, S. Yang, J. Xu, Y. Zhong *et al.*, "Exosomes-loaded electroconductive nerve dressing for nerve regeneration and pain relief against diabetic peripheral nerve injury," *Bioact. Mater.* **26**, 194–215 (2023).
- <sup>52</sup>S. Song, Q. Wang, Y. Qu, W. Gao, D. Li, X. Xu *et al.*, "Pregabalin inhibits purinergic P2Y2 receptor and TRPV4 to suppress astrocyte activation and to relieve neuropathic pain," *Eur. J. Pharmacol.* **960**, 176140 (2023).